Engineering Structures 289 (2023) 116245

Contents lists available at ScienceDirect

Engineering Structures

journal homepage: www.elsevier.com/locate/engstruct

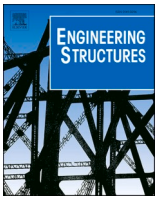

Nonlinear behaviour of corrosion damaged low-strength short reinforced concrete columns under compressive axial cyclic loading

Hammed O. Aminulai [a], Andrew F. Robinson [b], Neil S. Ferguson [c], Mohammed M. Kashani [d,*]

[a] University of Southampton, Boldrewood Innovation Campus, Burgess Road, Building 178, Southampton SO16 7QF, United Kingdom
[b] Testing and Structures Research Laboratory (TSRL), Building 178, University of Southampton, Boldrewood Innovation Campus, Burgess Road, Southampton SO16 7QF, United Kingdom
[c] Highfield Campus, University Road, Building 13 SO17 1BJ, United Kingdom
[d] University of Southampton, Boldrewood Innovation Campus, Burgess Road, Roomr 4019, Building 178, Southampton SO16 7QF, United Kingdom

ARTICLE INFO

Keywords:
Cyclic loading
RC column
Confinement
Corrosion
Seismic detailing
Ductility

ABSTRACT

New codes have recently introduced seismic detailing for new structures. However, there are still older reinforced concrete (RC) structures without proper ductile detailing for earthquake resistance in seismic-prone areas. These structures are further impacted by the corrosion of their embedded reinforcing bars, which further reduces the strength and ductility under axial cyclic loading. This paper summarises the results of an experimental investigation performed on low-strength short RC columns, with different confinement configurations, subject to varying degrees of corrosion to investigate their structural responses to axial cyclic loading. The experiment was conducted on 30 short RC columns (square and circular) with three levels of confinement and steel reinforcement corrosion loss ranging from 0% to ~ 30% subjected to cyclic compressive loading. The test results show that corrosion and inadequate confinements have a significant negative impact on the structural responses of corroded columns.

1. Introduction

Reinforced concrete (RC) columns are commonly used to construct civil engineering structures. They are affected by factors such as dry and wet cycles, freeze–thaw cycles, ageing of the materials, and the corrosion of reinforcement steel [1,2]. Among all these factors, steel corrosion has been reported to be the most devastating, with chloride-induced corrosion the most severe, leading to catastrophic failure and collapse of structures [3]. Corrosion exerts pressure on the interface between the reinforcement and concrete, leading to cracks and spalling of the cover concrete, thereby undermining the RC member's strength and ductility and reducing the structure's life span and long-term performance [4–6].

The corrosion of reinforcement in RC members significantly degrades their structural performance. It leads to structures with reduced load-carrying capacity, ductility, cracking and spalling of the concrete cover resulting in the structures losing their serviceability and structural safety [7]. Furthermore, corrosion significantly reduces the confinement effectiveness of the transverse reinforcement and the buckling resistance of longitudinal reinforcement in RC columns, especially structures in severely corrosive environments and subjected to seismic loading [2].

Numerous old RC bridges in marine environments and cold regions (using de-icing salt) suffer from steel corrosion resulting in the durability degradation of such bridges [8,9]. Furthermore, the corrosion of steel in bridge columns/piers leads to a reduction in performance degradation, such as a reduction of the load-carrying capacity of the columns/piers due to mass loss and strength deterioration of steel reinforcements [10–13], softening and spalling of the cover concrete [14,15], strength deterioration of the core concrete [16,17], and bond strength reduction between the steel reinforcements and concrete [9,18]. In addition, these bridges are designed with the old structural building codes without proper confinement detailing and seismic resistance, making them vulnerable to collapse under seismic excitation.

In recent years, the seismic response of corroded RC bridges in moderate-to-high seismic regions has been investigated [8,9,19,20]. The RC columns in the marine environment are severely affected by longitudinal and transverse reinforcement corrosion, which significantly impacts the hysteretic behaviour, loading capacity, energy dissipation and displacement ductility [21,22]. Guo et al. [23] stated that the

* Corresponding author.
E-mail addresses: h.o.aminulai@soton.ac.uk (H.O. Aminulai), a.robinson@soton.ac.uk (A.F. Robinson), nsf@isvr.soton.ac.uk (N.S. Ferguson), mehdi.kashani@soton.ac.uk (M.M. Kashani).

https://doi.org/10.1016/j.engstruct.2023.116245
Received 23 January 2023; Received in revised form 4 April 2023; Accepted 28 April 2023
Available online 14 May 2023

Table 1
Experimental test matrix of the RC columns.

Circular columns			Square columns		
Specimen label	Confinement level	Targeted corrosion (%)	Specimen label	Confinement level	Targeted corrosion (%)
C5A0	5	0	S5A0	5	0
C5A5	5	5	S5A5	5	5
C5A10	5	10	S5A10	5	10
C5A20	5	20	S5A20	5	20
C5A30	5	30	S5A30	5	30
C8A0	8	0	S8A0	8	0
C8A5	8	5	S8A5	8	5
C8A10	8	10	S8A10	8	10
C8A20	8	20	S8A20	8	20
C8A30	8	30	S8A30	8	30
C13A0	13	0	S13A0	13	0
C13A5	13	5	S13A5	13	5
C13A10	13	10	S13A10	13	10
C13A20	13	20	S13A20	13	20
C13A30	13	30	S13A30	13	30

Table 2
Reinforcements details for the circular columns.

Column type	Longitudinal reinforcement			Transverse reinforcement		
	Diameter (mm)	Number in column	Reinforcement ratio (%)	Diameter (mm)	Spacing (mm)	Volumetric ratio (%)
High confined ($L/D = 5$)	10	5	5.1	6	50	2.28
Medium confined ($L/D = 8$)	10	5	5.1	6	80	1.43
Low confined ($L/D = 13$)	10	5	5.1	6	133.33	0.86
High confined ($L/D = 5$)	10	4	3.21	6	50	1.18
Medium confined ($L/D = 8$)	10	4	3.21	6	80	0.74
Low confined ($L/D = 13$)	10	4	3.21	6	133.33	0.44

seismic performance of bridge piers in marine environments and earthquake-prone regions showed noticeable damage with an increase in the corrosion level on RC bridge columns. Meda et al. [21] performed quasi-static tests on two rectangular RC columns. They found that corroded columns' ultimate loading and displacement capacities decreased significantly, with a corrosion level of 20%. Ma et al. [24] experimentally investigated the seismic behaviour of 13 circular RC columns with corrosion damage under axial cyclic loading. The experimental results demonstrated that increasing corrosion decreased the loading capacity, stiffness, ductility and energy dissipation capacity. However, it was also found that the corroded specimens had almost the same energy dissipation capacity at the same displacement excursions when the mass loss was less than 14%.

In the literature, the effects of corrosion on the mechanical properties and deterioration of reinforcement have been well studied [25–28]. Also, the behaviour of RC beams with corroded reinforcement has also been well investigated, particularly their flexural and shear strength deteriorations owing to reinforcement corrosion [16,29–32]. Conversely, very little research has been done on the experimental investigation of the effects of any degradation on the performance of low-strength concrete RC columns subjected to seismic loading. However, several studies have been done on the impact of corrosion on the seismic capacity of RC columns that fail in flexure [21,33,34]. In contrast, others investigated the effectiveness of strengthening RC columns after axial cyclic loading [5,35,36].

There have been several studies to investigate the mechanical response of RC columns in seismic region to loading [35,37–39]. Some of these studies are on pristine columns subject to the combine effect of axial and lateral cyclic load [37,40–42] while others are numerical work to predict the mechanical behaviour of corroded bars in RC columns [43–45]. These works were able to predict the responses of RC columns but due to the complexity involve in the actual occurenece and quantification of corrosion in RC structures there are needs to actually conduct experimental tests to compare the mechanical response of RC columns in seismic region with the numerical data.

The previous experimental investigations are mostly on normal and high-strength concrete, but there are many old and ageing bridges/structures with low-strength columns/piers and improper confinement based on the old design in earthquake-prone regions. The effect of corrosion and inadequate confinement on such weak and old columns needs to be adequately investigated to understand their response to axial cyclic loading. In addition, there is a shortfall in research on the seismic performance of ageing RC short columns with low concrete strength subject to the combined effect of corrosion and varying confinement levels, particularly in investigations on their load-carrying and deformation capacities.

1.1. Research contribution and novelty

Cyclic experimental testing constitutes an effective method to provide insight into the seismic performance of the structural component. However, although it is recognised that corrosion-induced damage on coastal bridge piers significantly affects the safety of the structures during the long-term service period [23], the damage mechanism and the mechanical behaviour low-strength concrete are still not well understood. This paper investigates the effect of corrosion and confinement on the nonlinear cyclic behaviour of ageing low-strength RC columns.

Corrosion of reinforcement significantly affects the nonlinear response of bridge piers/columns subject to seismic and axial loadings, where the buckling of vertical bars in plastic hinge regions is the governing parameter. It is well known that bending moment combined with axial compression force will induce considerable strain on the edge of a section, and large tensile strains followed by high compression will bring the reinforcing bars to buckle and the concrete to crush or spall [46]. Reinforcement buckling inside RC structures is a more complex phenomenon than buckling of bare reinforcing bars. Recent studies have shown that multiple local parameters influence the buckling response of reinforcing bars inside RC structures compared to a plain reinforcing bar [47–49]. The buckling response of bars inside RC members primarily

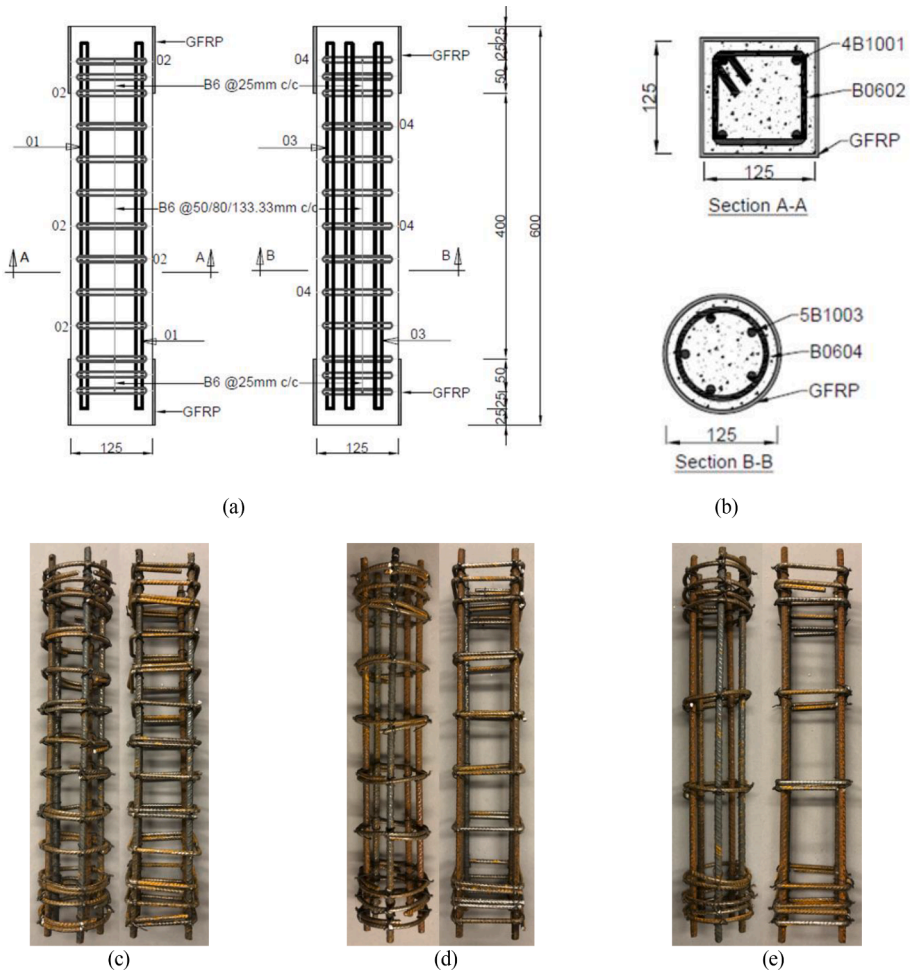

Fig. 1. RC columns details; (a) Elevetion (b) Cross sections (b) High confined (L/D = 5) reinforcement cages (c) Medium confined (L/D = 8) reinforcement cages (d) Low confined (L/D = 13) reinforcement cages.

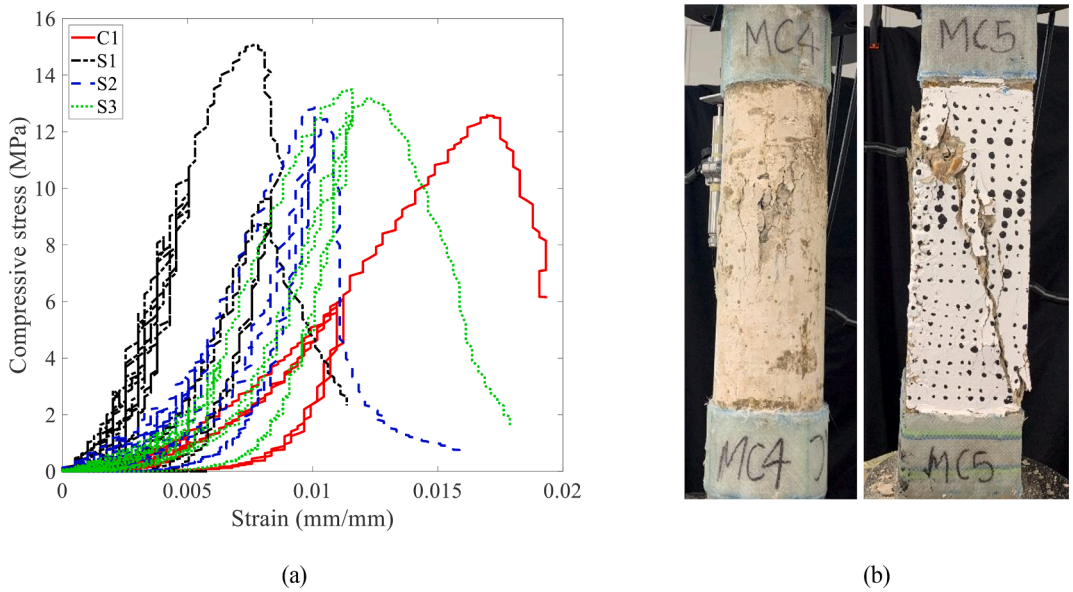

Fig. 2. Mass concrete behaviour (a) stress–strain response (b) observed failure after test.

depends on the resistance offered by the cover concrete and transverse reinforcement to bars against buckling.

While several studies have been dedicated to investigating the structural vulnerability of corrosion-damaged RC members, there is significant paucity in the literature on the influence of corrosion damage, confinement levels and cross-sectional shape on the seismic

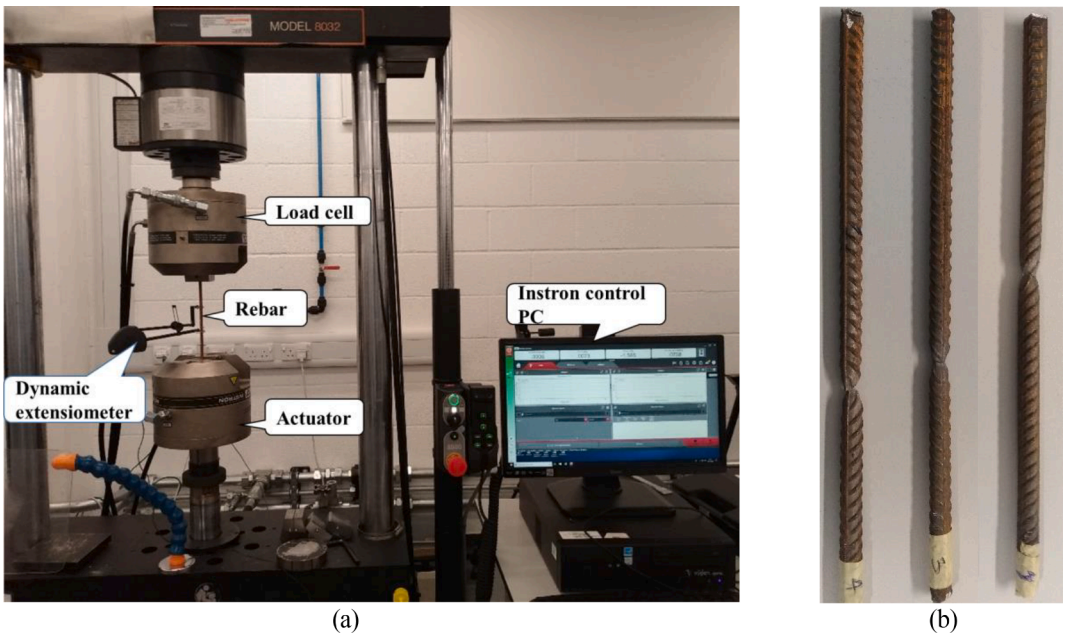

Fig. 3. Tensile test of rebars (a) experimental setup (b) observed failure of 10 mm bars.

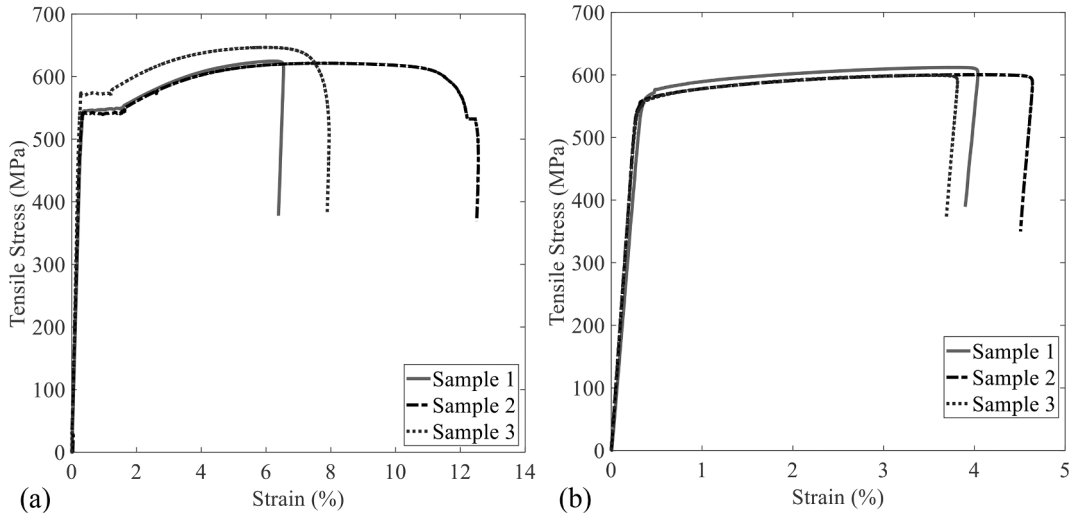

Fig. 4. Stress–strain behaviour of reinforcement bars (a) longitudinal (b) transverse.

Table 3
Mechanical properties of the uncorroded transverse and longitudinal bars.

Reinforcement type	10 mm	6 mm
Yield Strength, f_y (MPa)	551.68	531.82
Ultimate strength, f_u (MPa)	630.11	603.05
Modulus of Elasticity, E (GPa)	196.73	185.23
Yield Strain, $\varepsilon_y = f_y/\mathbf{E}$	0.00280	0.00287
Ultimate strain, ε_u	0.06349	0.03356
Strain ratio, $(\varepsilon_u/\varepsilon_y)$	22.67	11.69
Strength ratio, $f_u/f_y)$	1.142	1.134
Total elongation at maximum force, (%)	6.35	3.36
Total elongation at failure, λ_f (%)	8.49	4.16
Unit mass, m (kg/m)	0.624	0.224

behaviour of ageing RC bridge columns/piers. Several numerical and analytical models have investigated the effects of corrosion and transverse reinforcement confinements on seismic performance and failure modes of RC members with normal strength concrete [47,48,50,51]. However, they have not investigated ageing RC members with low-strength concrete. Therefore, there is a need for experimental investigation of the nonlinear cyclic response of corroded low-strength RC columns with various confinement ratios under cyclic compressive loading.

Axial cyclic behaviour of short columns is important in developing uniaxial constitutive models for corrosion damaged concrete (with various confinement), which can be used in modelling nonlinear seismic behaviour of corroded structures. Hence, the present study investigates, for the first time, the nonlinear behaviour of low-strength circular and square RC columns under simultaneous reinforcement corrosion, confinement configurations and cyclic compressive load. Five different degrees of reinforcement corrosion (i.e., 0%, 5%, 10%, 20% and 30%) with three confinement ratios based on the spacing of the transverse reinforcements are investigated under cyclic compressive load. The confinement ratios are assigned through the centre-to-centre spacing of the transverse reinforcement (L) and the diameter of the longitudinal reinforcement (D), known as the spacing-diameter, L/D ratio. Hence for

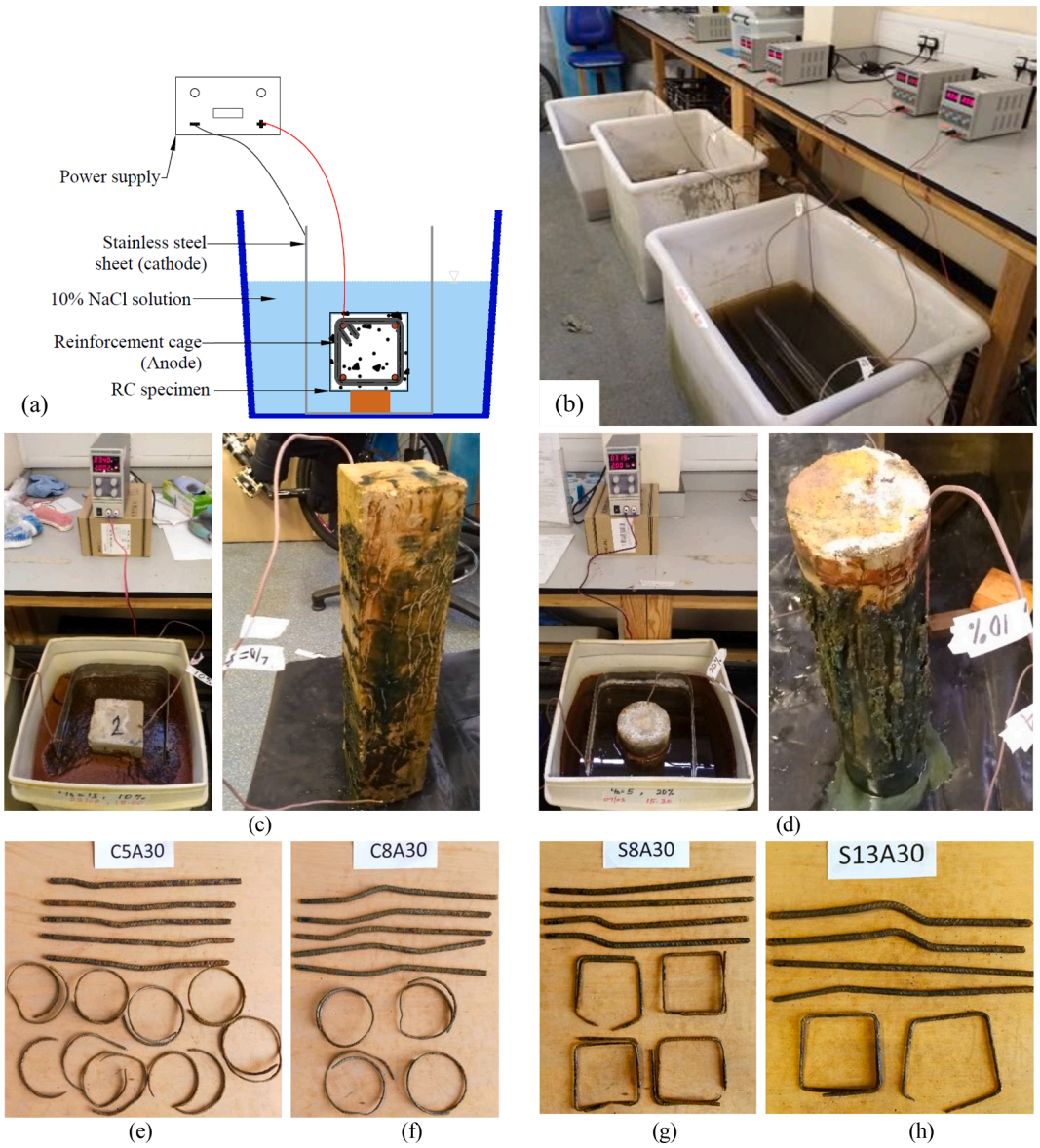

Fig. 5. Accelerated corrosion procedure; (a) Schematic setup drawing, (b), (c) and (d) laboratory setup and corroded columns after completion of corrosion, and (e-h) corroded rebars after cleaning.

the test, the three confinement ratios are: high ($L/D = 5$), medium ($L/D = 8$) and low ($L/D = 13$). The accelerated corrosion technique obtained different degrees of reinforcement corrosion. The failure modes of the RC columns, the load-deformation responses of RC columns and the inelastic buckling of the longitudinal reinforcements were analysed.

2. Experimental campaign

2.1. Specimen preparation and material characterisation

Thirty circular and square RC columns were cast and reinforced with British standard B500B ribbed thread steel bars. The configurations for the experimental test samples are presented in Table 1. The square samples have a 125 × 125 × 600 mm dimension incorporating 4 No. 10 mm diameter longitudinal bars, while the circular samples (125 mm diameter and 600 mm long) have 5 No. 10 mm longitudinal bars (Table 2). The RC columns are designed with three different confinement; high ($L/D = 5$), medium ($L/D = 8$) and low ($L/D = 13$) in the middle 400 mm zone, while the top and bottom (100 mm) ends have closely spaced (25 mm) transverse bars (Fig. 1(a-e)). The higher the spacing-diameter ratio (L/D), the lesser the RC columns' confinement effectiveness and load-carrying capacity. Furthermore, each column has different corrosion levels designated as 0%, 5%, 10%, 20% and 30% (Table 1). The 100 mm ends of the columns were wrapped with layers of epoxy-resin-soaked glass fibre-reinforced polymer (GFRP), using the wet layup technique to minimise the stress concentration at the ends of the columns and ensure that the failure occurs at the RC columns' middle zone.

The concrete mix was designed as low-strength concrete, representing ageing columns with an estimated mean compressive strength of 20 MPa and a maximum aggregate size of 10 mm. All the columns were cast with a 10 mm nominal concrete cover. Concrete samples with the same configuration as the square and circular columns were collected during the casting to determine the actual compressive strength of the concrete. The compressive strength test was done at the Testing and Structures Research Laboratory (TSRL), University of Southampton using the servo-hydraulic 630 kN Instron Schenk machine. The concrete columns were tested using the axial cyclic loading protocol with displacement control at a constant loading rate of 0.1 mm/sec until failure. Fig. 2(a) shows the stress–strain response of the unreinforced

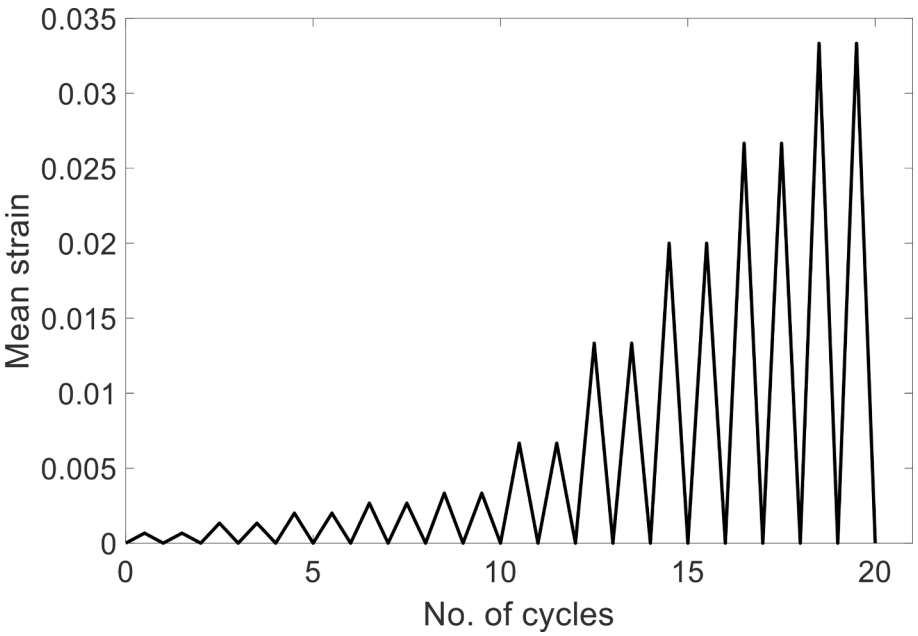

Fig. 6. Cyclic compressive loading protocol.

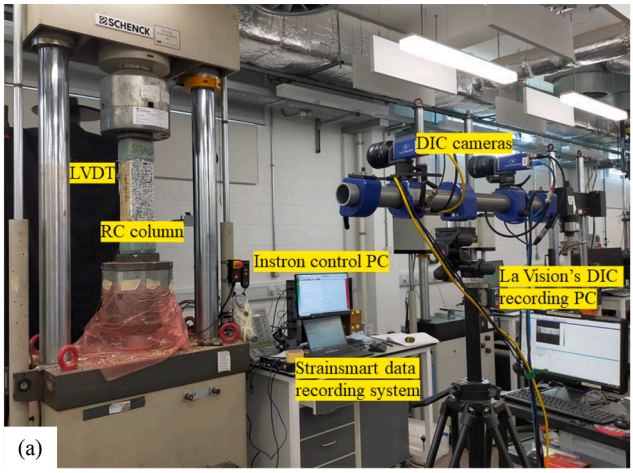

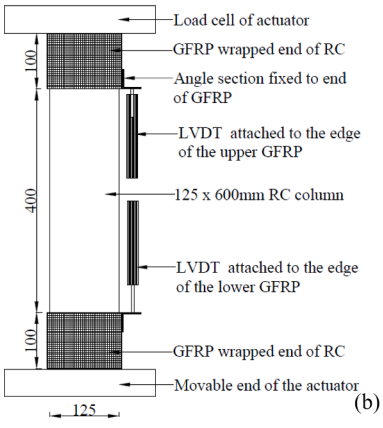

Fig. 7. Experimental test setup (a) laboratory setup; (b) schematic of the LVDT connection; (c) Image of the LVDT connections to the RC samples and (d) RC sample with speckles for DIC processing.

Table 4
DIC processing parameters.

Technique used	3D (Stereo) DIC
Camera name	Imager E-lite 5 M
Focal length	28.4621 mm
RMS of fit	0.303396 pixel
Size of dewarped image	1961 × 2479 pixel
Subset	53
Step	17
Correlation criterion	ZNSSD
Shape function	Quadratic
Interpolation function	Bicubic splines
Strain	
Smoothing method	Polynomial - Bilinear
Resolution	3.45 mm
Calculation mode	accurate

concrete samples with the square samples (S1, S2 and S3) having an average compressive strength 13.8 MPa while the circular sample (C1) has 12.6 MPa. Furthermore, the mass concretes columns show similar failure patterns having diagonal cracks at the middle of the column (Fig. 2(b)).

Tensile tests were conducted on samples of 10 mm, and 6 mm rebars using the servo-hydraulic (Instron 8032) test machine with 100kN capacity and ± 50 mm travel to determine the mechanical properties. Three reinforcement samples were selected for the tensile tests according to BS EN 10080:2005[52]and BS 4449:2005 + A3:2016[53]. In addition, the rebars were subjected to different loading rates before and after the yielding as specified in BS EN ISO 6892–1:2019[54]. The corresponding strain resulting from the loading was measured with a 50 mm dynamic extensometer (±5mm maximum stroke) attached to the rebar. Fig. 3(a) shows the experimental setup of the tensile test, while Fig. 3b shows the failed rebar after the test.

The stress–strain response of the rebars is shown in Fig. 4, while the summary of the mechanical properties is shown in Table 3. The average yield, ultimate strengths, and strain values obtained conform to the values specified for B500B rebars [53]. Also, the variation in unit mass from the code specification for the rebars is 0.9% and 1.13% for the 6 mm and 10 mm bars, respectively and are considered insignificant[55].

2.2. Accelerated corrosion simulation

Reinforcement corrosion is commonly obtained by two methods, i.e. natural corrosion and electrochemical corrosion [56]. The natural corrosion of reinforcing bars in the laboratory will last too long (continuously for several years or longer), which is impractical for a laboratory with limited space [57]. Therefore, electrochemical corrosion with an appropriate and constantly direct current is applied for accelerating laboratory testing and has been proved to have a similar result as natural corrosion [56,58,59]. The constant external current method has been used by several researchers to successfully induce the accelerated corrosion of reinforcing bars in RC samples [4,24,55,60].

The corrosion of the RC columns was accelerated in the laboratory by submerging them in a 10% sodium chloride solution and passing direct current through it using the DC power supply. The positive node of the power supply is connected to the reinforcement cage, while the negative node is connected to the stainless steel sheet wrapped around the submerged RC column (Fig. 5(a - d)). The DC power supply was adjusted to

Table 5
Accelerated corrosion parameters for circular RC columns.

Specimen No.	Corrosion current density (mA/cm^2)	Corrosion duration (days)	Estimated mass loss (Eq. (3) (%)	Measured mass loss of longitudinal bars (Eq. (4) (%)	Measured mass loss of transverse bars (Eq. (4) (%)
C5A0	0	0	0	0	0
C5A5	1.00	3.0	5	4.4	11.2
C5A10	1.00	6.0	10	5.2	21.1
C5A20	1.00	12.1	20	14.4	37.9
C5A30	1.00	18.1	30	19.1	54.0
C8A0	0	0	0	0	0
C8A5	1.16	2.7	5	6.5	13.2
C8A10	1.16	5.4	10	9.8	23.5
C8A20	1.16	10.8	20	12.4	46.0
C8A30	1.16	16.2	30	26.3	51.4
C13A0	0	0	0	0	0
C13A5	1.28	2.5	5	9.3	15.5
C13A10	1.28	5.0	10	11.1	20.4
C13A20	1.28	10.0	20	18.5	36.0
C13A30	1.28	15.0	30	23.7	50.7

Table 6
Accelerated corrosion parameters for square RC columns.

Specimen No.	Corrosion current density (mA/cm^2)	Corrosion duration (days)	Estimated mass loss (Eq. (3) (%)	Measured mass loss of longitudinal bars (Eq. (4) (%)	Measured mass loss of transverse bars (Eq. (4) (%)
S5A0	0	0	0	0	0
S5A5	0.99	2.9	5	4.3	13.0
S5A10	0.99	5.8	10	5.7	17.0
S5A20	0.99	11.7	20	12.1	36.4
S5A30	0.99	17.5	30	15.9	49.2
S8A0	0	0	0	0	0
S8A5	1.17	2.6	5	5.7	17.0
S8A10	1.17	5.1	10	8.8	18.0
S8A20	1.17	10.2	20	12.5	34.0
S8A30	1.17	15.3	30	14.2	39.1
S13A5	0	0	0	0	0
S13A5	1.33	2.3	5	5.9	11.3
S13A10	1.33	4.6	10	10.2	21.1
S13A20	1.33	9.3	20	16.8	28.7
S13A30	1.33	13.9	30	24.4	48.5

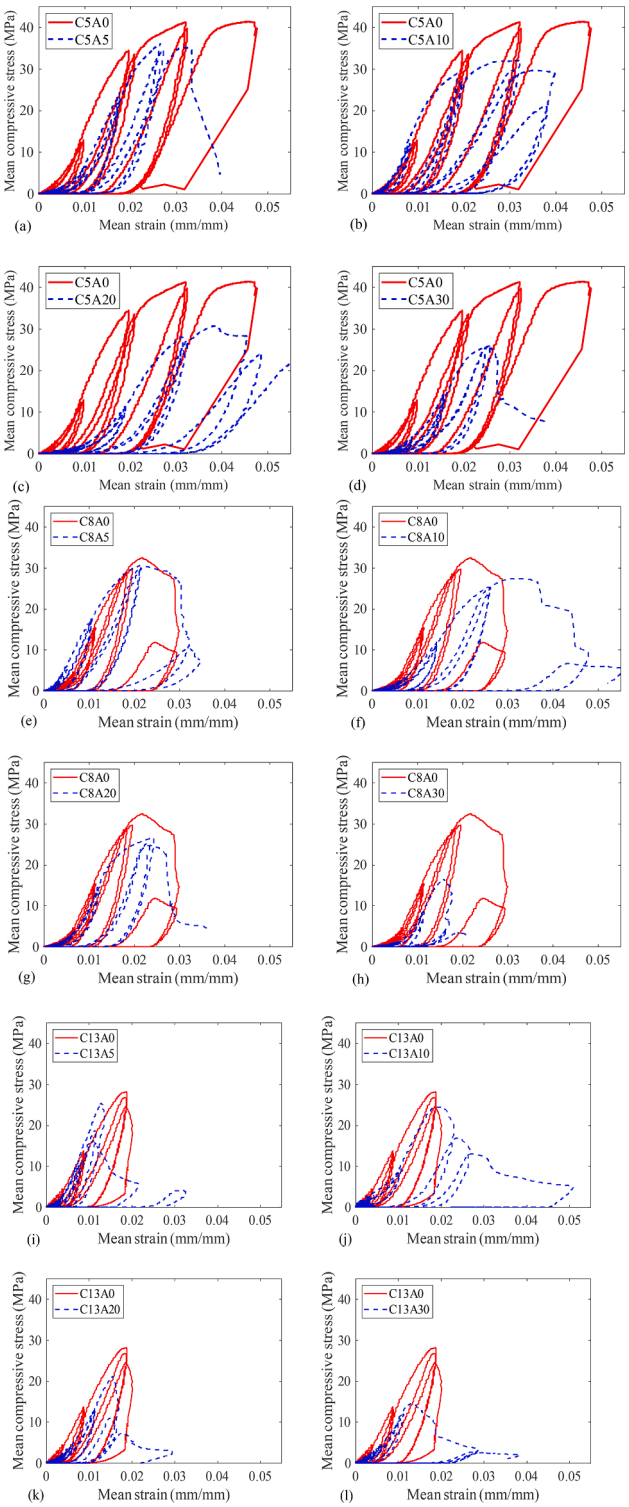

Fig. 8. Axial cyclic stress–strain response of circular columns; L/D = 5 (a-d), L/D = 8 (e-h) and L/D = 13 (i-l).

supply a constant current of 2Amp for the corrosion of the rebars. The duration for the expected mass loss was estimated using Faraday's 2nd law of electrolysis [55] as follows:

$$m_l = \left(\frac{M}{Z}\right)\left(\frac{Q}{F}\right) \tag{1}$$

where m_l is the estimated mass loss (g), M is the molar mass of the iron (56 g/mol), Z is the ionic charge for iron (valence electron transferred per ion = 2), and F is the Faraday's constant (96500C/mol). Q is the total electric charge passed through the element and is calculated from Eq. (2) as:

$$Q = \int_0^T Idt = IT \tag{2}$$

where I is the magnitude of the applied current (Ampere, A), T is the

Fig. 9. Observed failure modes of circular columns with the different corrosion levels and confinement ratios; L/D = 5 (a - e), L/D = 8 (f - j) and L/D = 13 (k - o).

estimated time to achieve the desired corrosion (s). Combining equations (1) and (2) gives the estimated mass loss as:

$$m_l = \frac{MIT}{ZF} \tag{3}$$

Equation (3) gives an approximate estimate of the expected corrosion mass loss, primarily different from the actual corrosion mass loss obtained after the corrosion process. Hence, the corroded bars are removed from the RC columns after testing and cleaning to determine the exact mass loss resulting from the corrosion of the sample. First, the rebars were cleaned by soaking them in vinegar and afterwards using a wire brush to remove the surface's concrete and rust particles per ASTM G1-03 [61]. This brushing and cleaning procedure was also applied to the uncorroded specimen, and the effect of brushing is negligible on the mass loss of the base materials [55,62,63]. The actual mass loss due to corrosion is afterwards determined by weighing the rebars and is estimated from Equation (3):

$$\gamma = \frac{m_0 - m}{m} \times 100 \tag{4}$$

where m_0, gives the mass per unit length of the uncorroded rebar, and m, is the mass per unit length of the rebar after cleaning. This equation provides an average corrosion loss (mass loss) along the length of the rebar.

2.3. Axial cyclic loading protocol and instrumentation

The RC columns were tested under axial compressive axial cyclic loading. The loading protocol was set to have 20 cycles with ten different mean strains, each strain peak repeating twice, as shown in Fig. 6. The mean strain was estimated from the displacement values of a similar experimental test done on corroded RC under monotonic loading. The load was applied using the displacement control condition using the servo-hydraulic Instron Schenck 630 kN testing machine within TSRL. The first five lower strain peaks were applied at 0.1 mm/sec loading rate while the remaining strain peaks were at 0.15 mm/sec. The axial cyclic loading protocol was setup using the Instron Wavematrics software [64]. The RC columns were tested under axial cyclic compressive load using the displacement control with a lower loading rate for the first ten cycles while the remaining cycles were at a slightly higher rate. Also, the test was conducted under complete axial cyclic compression loading, with each loading cycle repeated twice without going into the tension loading zone. The servo-hydraulic machine used an internal Linear Variable Differential Transformer (LVDT) that measures the displacement of the actuator during loading. In contrast, a load cell measures the corresponding load resulting from the applied displacement. The setup of the experiment is presented in Fig. 7(a).

The displacement at the middle 400 mm zone of the RC columns is measured with the LVDTs fixed to the edge of the Glass fibre-reinforced

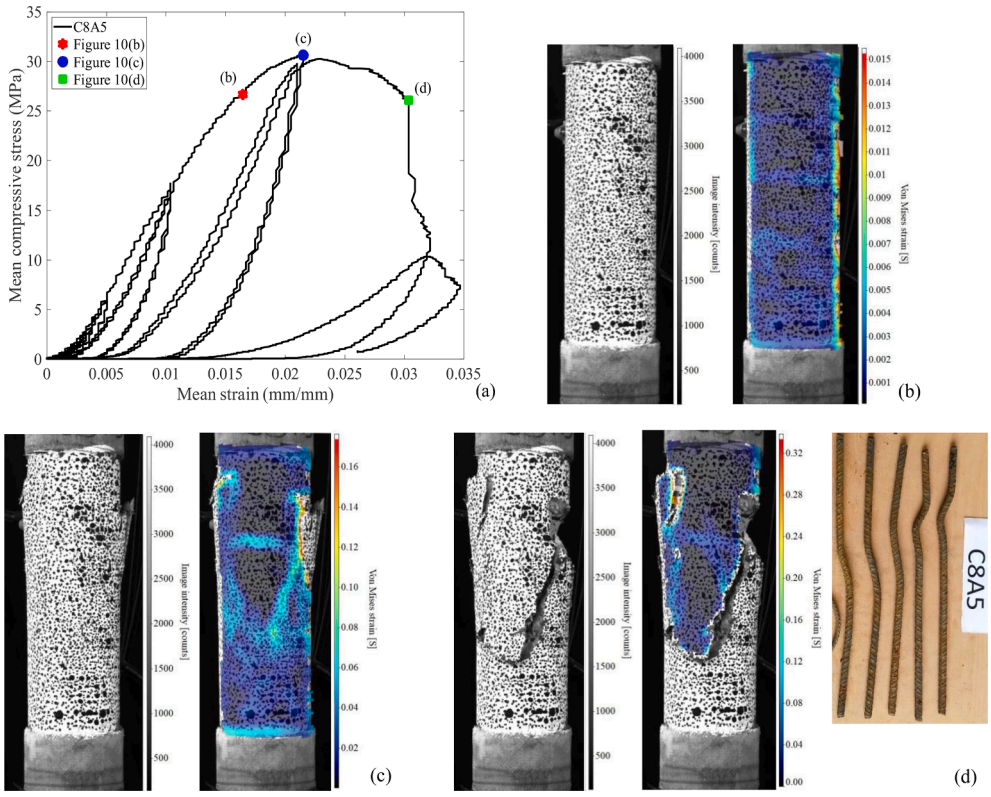

Fig. 10. Processed DIC images of circular column (a) stress–strain response showing location of processed images (b) at yield stress, (c) at ultimate stress and (d) between ultimate stress and collapse.

polymers (GFRP) strengthened ends and the stereo 3D Digital Image Correlation (DIC). The two LVDTs with 50 mm strokes were fixed such that they touch the angle irons fixed to the edge of the Glass fibre-reinforced polymers (GFRP) strengthened ends of the RC columns (Fig. 7(b) and 7(c)). This ensures that the LVDTs measure the axial deformations in the middle 400 mm section of the columns, which are recorded via a multichannel data acquisition unit (Strainsmart 8000).

A digital image correlation (DIC) is a non-destructive non-contact full-field optical measurement technique capable of capturing digital images of the surface of an object to obtain the in-plane strains and out-of-plane deformations in its 2D and 3D configurations. The DIC was used simultaneously with the LVDTs to capture the crack propagation and deformations at the 400 mm middle section of the RC columns under compressive load. The video imaging is performed using LaVision's Davis imaging software involving two cameras (Imager E-Lite 5 M) fitted with Nikon AF Nikkor 28 mm f/2.8D (28 mm focal length and 2.8 maximum aperture) lenses (Fig. 7(a)). The cameras were calibrated to capture the RC column's out-of-plane and vertical displacements during loading using the dots marked on the columns (Fig. 7(d)). The images recorded are further processed using LaVision's Davis 10 software to see the strain distribution resulting from the applied loading. The parameters used in the DIC image acquisition and processing are presented in Table 4.

3. Experimental results and discussion

3.1. Calculation of corrosion and mass loss ratio

The actual mass losses resulting from the corrosion of the reinforcements are estimated using Eq. (4) and are illustrated in Tables 5 and 6 for the circular and square columns, respectively. The results indicate that the stirrups rebars had more severe corrosion than the longitudinal bar under the same constant current and duration [38]. This mass loss results from the closeness of the transverse bars to the surface of the concrete, leading to a possibly higher concentration of chloride ions and an early start to the corrosion [65]. Furthermore, the diameter of the longitudinal rebar (10 mm) was greater than that of the stirrups (6 mm). In this regard, the mass loss ratio of transverse stirrups with smaller diameters was higher than that of the longitudinal rebar, according to Faraday's second law of electrolysis [55].

General and uniform corrosion is obtained by applying low current at a shorter duration, as applying low current at a more prolonged duration results in localised corrosion. Furthermore, using a higher current at a shorter duration also results in localised and pitting corrosion [66]. In this work, a constant current of 2A was used to accelerate the corrosion of the RC columns. This results in corrosion current densities and estimated mass losses in Tables 3 and 4, with the square columns having higher corrosion densities in the sparsely confined columns than the circular columns with similar configurations. Furthermore, the applied current density is close to the 1 mA/cm^2 recommended by Nguyen and Lambert [66] for the laboratory simulation of corrosion of steel embedded in concrete.

3.2. Axial cyclic testing of circular columns

The stress–strain responses of the circular columns to the applied axial compressive load are presented in Fig. 8 (a-l). These stress–strain responses were plotted from the LVDTs data since it shows the deformation of the 400 mm middle zone section rather than the readings from the machine load cell that captures the deformation of the whole column under loading. The cyclic responses of the corroded columns under loading were compared with the corresponding behaviour of the non-corroded columns in each confinement configuration.

The RC column samples all have similar stress–strain responses under axial cyclic load. The deformation started with minor vertical cracks, which subsequently enlarged with further loading, leading to

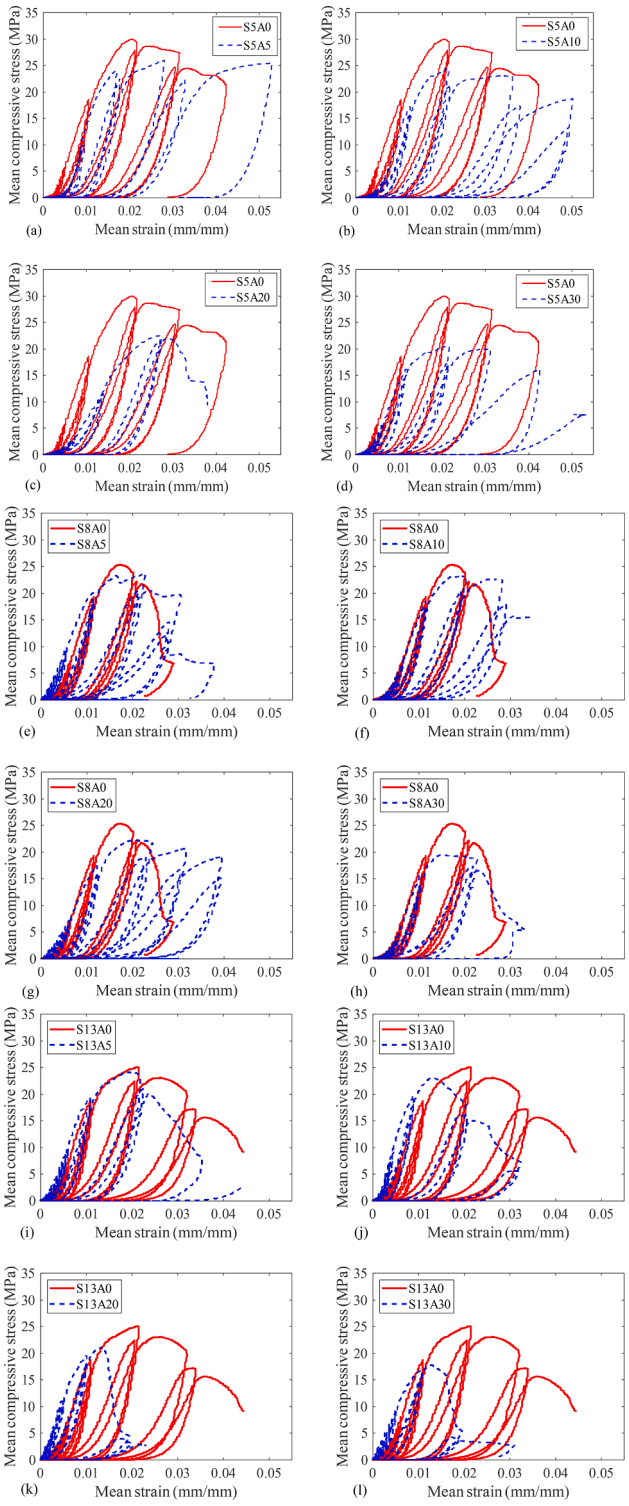

Fig. 11. Axial cyclic stress–strain response of square columns; L/D = 5 (a-d), L/D = 8 (e-h) and L/D = 13 (i-l).

spalling of the concrete cover as the longitudinal bars buckled due to lateral expansion of the RC columns. The observed cyclic responses of the RC columns are similar at the elastic range until yield and afterwards becomes nonlinear beyond the peak stress due to the corrosion and confinements of the rebars.

The hysteretic curve of the corroded columns within each confinement's configuration was compared with the non-corroded ones. It showed a gradual decrease in the strength, stiffness and ductility of the columns as the corrosion loss increased. The corrosion of longitudinal and transverse bars reduces the column's ultimate strength and load-carrying capacity. Consequently, columns with very close mass loss in the highly confined ($L/D = 5$) columns have their maximum strengths relative to each other, especially at low corrosion between 5% and 10% (Fig. 8(a - d)). For example, the strength loss between the highly confined (uncorroded and corroded) columns was reduced by 13%, 22%, 26%, and 37% for the 5%, 10%, 20% and 30% estimated mass loss,

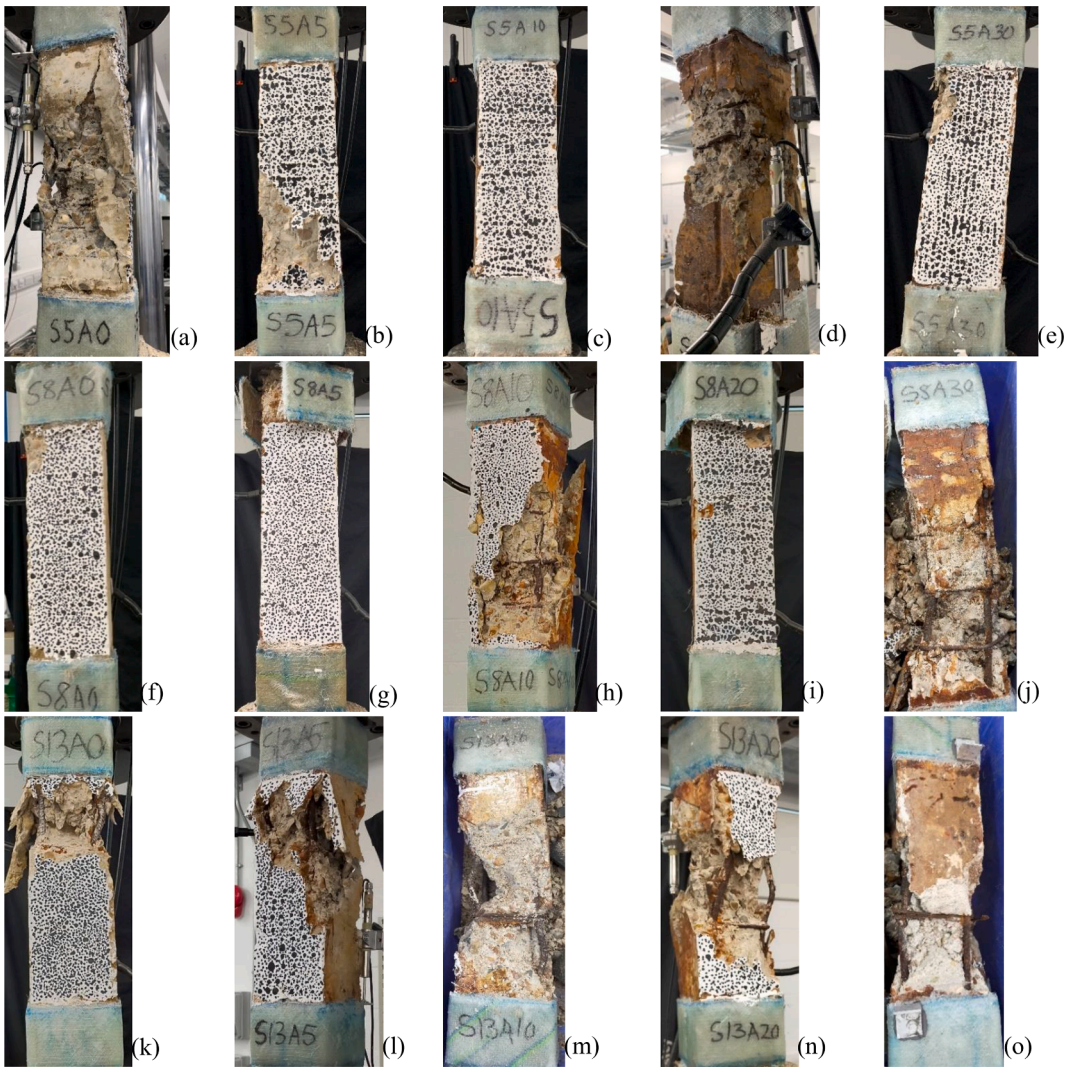

Fig. 12. Observed failure modes of square columns with different corrosion levels and confinement ratios; L/D = 5 (a - e), L/D = 8 (f - j) and L/D = 13 (k - o).

respectively. This trend is also observed in the medium ($L/D = 8$) with a strength reduction range between 5% and 50% (Fig. 8(e - h)) and low confined ($L/D = 13$) columns having between 10% and 48% reduction (Fig. 8(i - l)).

The applied cyclic compressive load results in the premature failure of some of the highly confined columns resulting from the GFRP failure at the top/bottom of the column (Fig. 9(a-d)). Furthermore, the applied load led to concrete cover spalling and hence buckling of the longitudinal bars and, in some cases, fracture of the transverse bar (Fig. 9(e, h and j)) in some columns. The longitudinal bars buckled mostly at the expected middle 400 mm zone, with some columns having shear buckling due to inadequate confinement (Fig. 9(k and o)), loss of confinement resulting from pitting corrosion (Fig. 9(j)), and the transverse bars' fracture (Fig. 9(h and i)).

The DIC tracks the RC columns' strain response and cracks damage to the applied compressive load. Fig. 10(a) shows the stress–strain response of one of the circular columns and the locations of the processed images (at yield stress, ultimate stress and beyond the ultimate stress). The processed images within the column's middle zone section showed the column's strain contour with the cracks, spalling of the cover concrete, and the buckling of the reinforcement captured. Fig. 10(b - d) are the Von Mises strain processed from the captured images during loading. These values correspond to the strain estimated from the LVDTs at yield stress, ultimate stress and beyond the ultimate stress.

The DIC image process showed that it could not adequately capture the crack propagation on the circular columns during testing due to the curvature of the column especially at lower load (Fig. 10(b)).

3.3. Axial cyclic testing of square columns

Similar to the circular columns, the stress–strain relationship showed identical behaviour within the elastic region in all the columns until the yield stress, beyond which the confinement configurations and increase in the corrosion degree resulted in a subsequent decrease in the load-carrying capacities. The stress–strain responses of the columns to the applied axial compressive load are presented in Fig. 11 (a-l). The cyclic responses of the corroded columns were compared with the corresponding behaviour of the non-corroded columns in each confinement configuration. The columns all have similar stress–strain responses under axial cyclic load. The deformation started with minor vertical cracks, which subsequently enlarged with further loading, leading to spalling of the concrete cover and, eventually, the buckling of the longitudinal bars.

The hysteretic curve of the corroded columns within each confinement's configuration was compared with the non-corroded ones. It showed a gradual decrease in the strength, stiffness and ductility of the columns as the corrosion loss increased. The strength of the RC columns decreased due to the combined effects of buckling the longitudinal bars and crushing the concrete. The corrosion of both longitudinal and transverse bars reduces the column's ultimate strength and load-

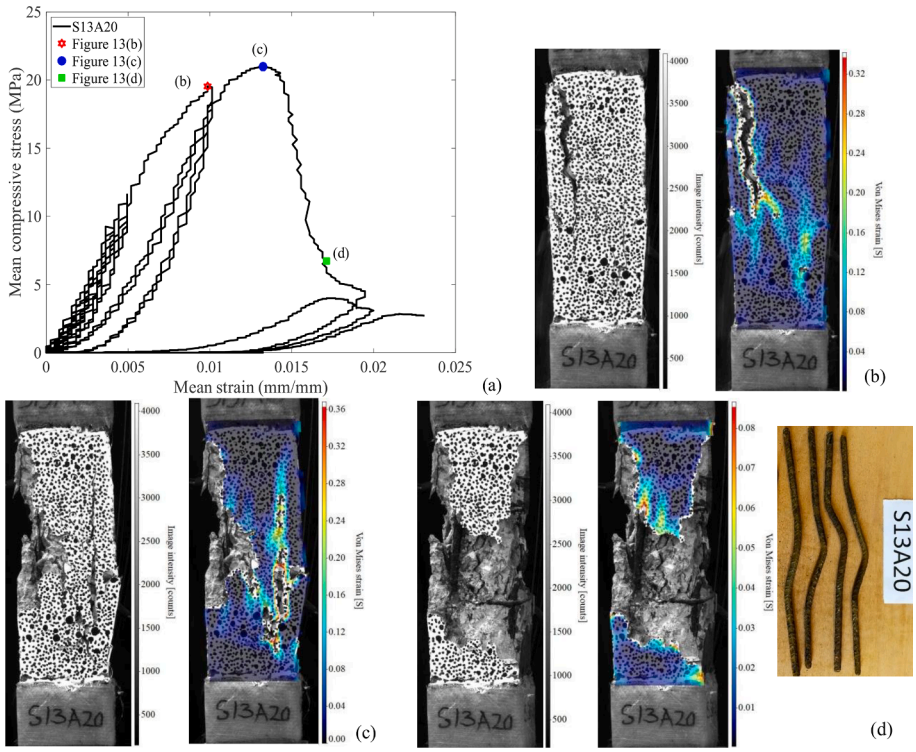

Fig. 13. Processed DIC images of square column (a) stress–strain response showing location of processed images (b) at yield stress, (c) at ultimate stress and (d) between ultimate stress and collapse with the buckling at the end of the test.

carrying capacity. Consequently, columns with very close mass loss in all the confinement configurations have their maximum strengths relative to each other, especially at low corrosion between 5% and 10% (Fig. 11 (a - l). The strength reduction from corrosion in the highly confined columns was 13%, 18%, 25%, and 31% for the 5%, 10%, 20% and 30% estimated mass loss, respectively. This trend is also observed in the mediumly confined columns ($L/D = 8$) with a strength reduction range between 7% and 23% (Fig. 11(e - h)) and low-confined columns ($L/D = 13$) having between 4% and 29% reduction (Fig. 11(i - l)).

Similar to the circular columns, the applied axial cyclic load results in the concrete cover's spalling (Fig. 12(b)), transverse bars fracture (Fig. 12(d and j)) and longitudinal bars buckling (Fig. 12(a, m, n and o)). Also, some of the non-corroded columns (0% corrosion) have failure of the strengthening GFRP at the top/bottom of the column (Fig. 12(c, f, g and i)), leading to stress concentration and premature failure of the ends of the columns. The failure of the GFRPs occurs due to the sharp edges of the square columns.

Fig. 13(a) shows the stress–strain response of one of the low, confined square RC columns with an estimated 20% corrosion mass loss. Fig. 13(b - d) are the processed images from the DIC at different locations during the compression testing on the column. The processed DIC images within the middle zone section of the column show the images with and without the strain contour on the column with the crack propagation, spalling of the cover concrete, and the reinforcement's buckling. Fig. 13(d) further shows the buckled longitudinal bars at the end of the test after removal and cleaning.

3.4. Impact of corrosion on cumulative energy dissipation capacity

Experimental studies on the cyclic behaviour of corroded beams and columns [8,24,67] showed that buckling and/or fracture of corroded bars significantly affects the global response and plastic rotation capacity and plastic hinging mechanisms of the corroded RC elements. Consequently, in the seismic assessment and evaluation of existing corroded structures, consideration needs to be given to the buckling of the rebars, even if the structure is designed initially to have sufficient confinement reinforcement.

The plots of the normalised accumulated hysteretic energy versus the number of cycles are presented in Fig. 14. The cumulative energy dissipated of each test specimen at each loading cycle is normalised against their corresponding total cumulative energy dissipated at failure. Fig. 14(a-c) shows the Influence of corrosion on the accumulated energy dissipation of circular RC columns with different confinement configurations. In contrast, Fig. 14(d-f) shows the impact of corrosion on the accumulated energy dissipation of square RC columns. The plots showed similar behaviour for all the columns with very low energy dissipated at the smaller cycles and a steep increase in the dissipated energy after the 10th cycle. The steep increase in the dissipated energy is more significant at high corrosion and low confinement in both the circular and square columns though the circular coumns have better energy dissipated. It should be noted that extensive corrosion lead to a large reduction in the energy dissipated by a column as such the highly corroded columns are more likely to have brittle failure than the uncorrodd columns [39].

3.5. Impact of corrosion on buckling of vertical reinforcement

Corrosion generally reduces the cross-sectional area of the bars available to sustain the applied load [68]. This reduction becomes more severe in bars with pitting corrosion, resulting in localised reduction in the cross-sectional areas of the bars, leading to rebar fracture and localised buckling [12]. The results of the tests on the corroded columns showed that the pitting effect is more significant, as it leads to the buckling mechanism and reduction in the load-carrying capacity of the column (Figs. 15 and 16). For instance, longitudinal bars in columns with $L/D = 5$ confinement (Figs. 15(a-c) and 16(a-c)) had less noticeable buckling failure, especially in the circular columns and at lower corrosion degrees than bars from the $L/D = 8$ and $L/D = 13$ configurations [55,68]. This buckling from the columns with $L/D = 5$ (Fig. 15(d)) rebars at higher corrosion levels results from the unsymmetrical cross-

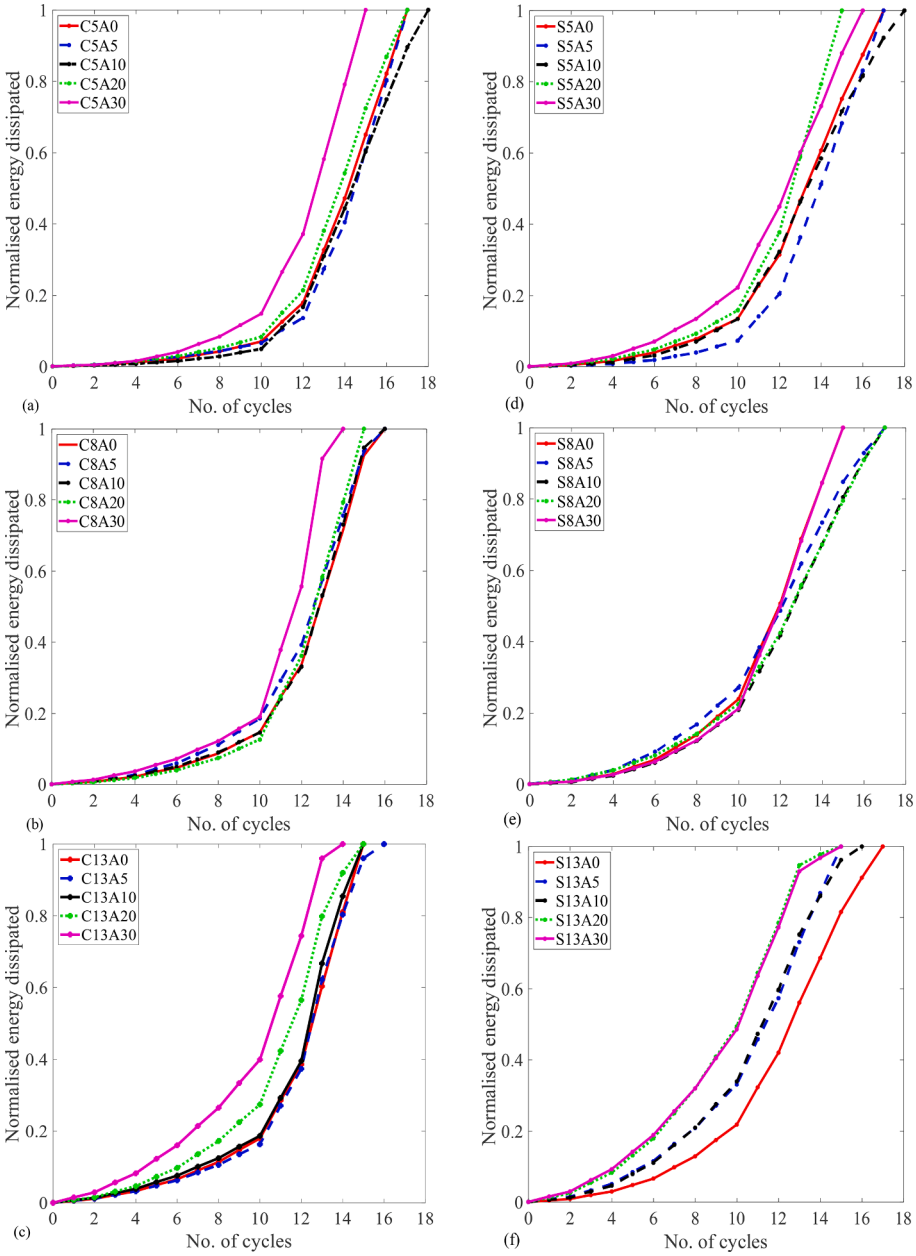

Fig. 14. Normalised dissipated energy of the RC columns; circular (a) L/D = 5, (b) L/D = 8 and (c) L/D = 13; square (d) L/D = 5, (e) L/D = 8 and (f) L/D = 13.

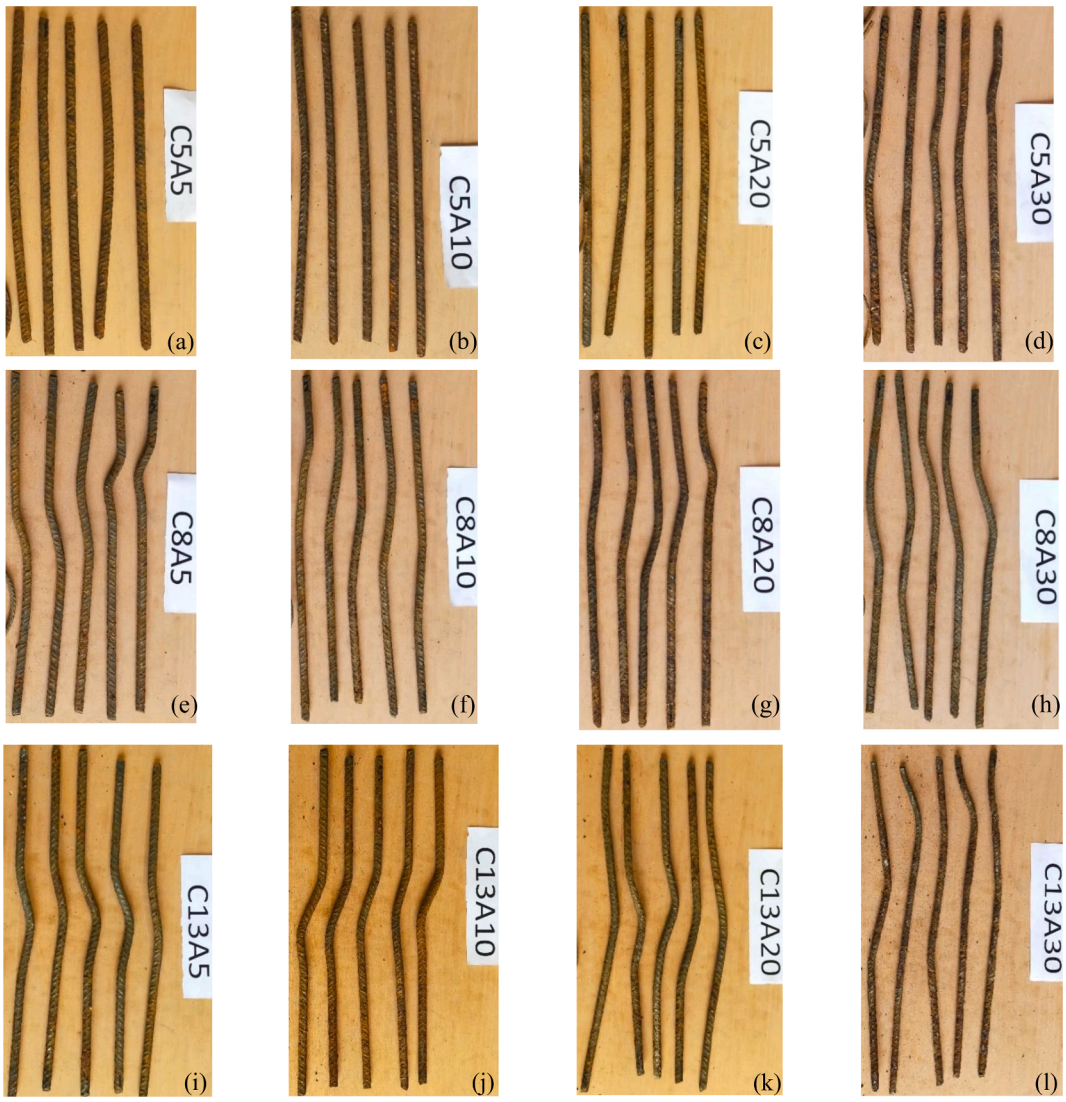

Fig. 15. Observed buckling failure of the longitudinal reinforcement in circular columns; L/D = 5 (a-d), L/D = 8 (e-h) and L/D = 13 (i-l).

sections arising from the pitting corrosion causing imperfections in the bar and leading to additional bending moment and local stresses at the pitted sections [12,55]. Meanwhile, the buckling from the columns with $L/D = 8$ and $L/D = 13$ results from the combination of pitting corrosion and inadequate confinement provisions leading to premature yielding and squashing of the weakest section even at lower corrosion degrees [69]. Those columns with more uniformly distributed corrosion and a relatively small mass loss showed similar behaviour to those with uncorroded bars with a more visible buckling at higher compressive load [55].

3.6. Impact of corrosion on the strength and strain of confined RC column

The strength loss resulting from the corrosion and confinement ratios of the RC columns is determined by normalising the ultimate strength of the corroded columns (σ_{ucorr}), to the ultimate strength of the pristine columns ($\sigma_{upristine}$). The normalised ultimate strength loss of the different confined RC columns is plotted relative to the percentage of corrosion mass loss. Afterwards, linear trend lines are fitted to the test data to estimate the strength reduction due to corrosion and confinement ratios. The R-square goodness of fit values obtained from the trend lines ranges from 0.78 to 0.96 for the circular columns at different confinement ratios (Fig. 17a), while the variation for the square columns is from 0.84 to 0.95 (Fig. 17b).

The ultimate strength of the confined corroded RC columns is reduced with an increase in the confinement degree and corrosion mass loss. For example, the well-confined circular columns with L/D = 5 (Fig. 17(a)) have a strength reduction range of 13.1%, 22.5%, 25.8% and 37.3% for the 4.4%, 5.2%, 14.4% and 19.1% corrosion mass loss, respectively. Also, the well-confined square columns with L/D = 5 (Fig. 17(b)) have a strength reduction range of 13.1%, 18.3%, 24.8% and 31.4% for the 4.3%, 5.7%, 12.1% and 15.9% corrosion mass loss, respectively. A similar trend is also observed in the mediumly confined (L/D = 8) and sparsely confined (L/D = 13) columns. The strength reduction increases with increased corrosion mass losses in the circular and square columns.

The axial strain variation of the confined RC columns to corrosion loss was also investigated by normalising the ultimate strain, i.e. strain at maximum stress, of the corroded columns (ϵ_{ucorr}), to the ultimate strain, i.e. strain at maximum stress, of the pristine columns ($\epsilon_{upristine}$). Fig. 17(c) and (d) show the circular and square column plots. The plot of the circular columns (Fig. 17c) generally indicates a reduction in the ultimate strain with an increase in the corrosion and confinement levels, except in some columns in the medium and low confined ranges with ultimate strain greater than their corresponding pristine column. This results from the failure of the GFRP ends, reducing the uncorroded

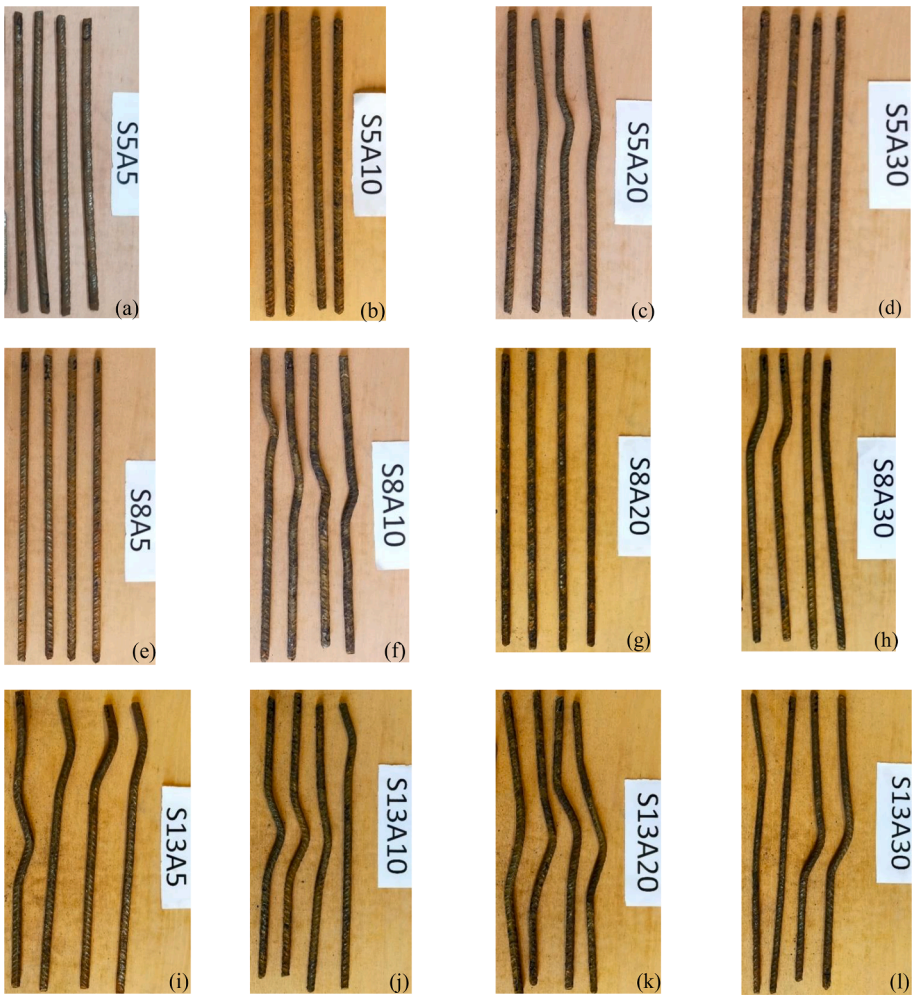

Fig. 16. Observed buckling failure of the longitudinal reinforcement in the square columns; L/D = 5 (a-d), L/D = 8 (e-h) and L/D = 13 (i-l).

columns' capacity under load.

4. Comparison of the response of circular and square columns

Fig. 18 (a-o) shows the normalised stress–strain response of the circular and square columns with similar confinement configurations and corrosion mass losses. First, the axial stress resulting from the loading of the columns is normalised against the ultimate strength of each column and plotted against the corresponding axial strain values. The columns show similar responses and stiffness within the elastic region until the peak strength is reached. Afterwards, the corrosion and confinement result in a loss of stiffness and reduced ductility of the RC columns [70,71].

Generally, the highly confined columns (L/D = 5) at the lower corrosion mass loss have a higher ductility (especially the square columns) than columns in the mediumly confined (L/D = 8) and lowly confined (L/D = 13) at the same corrosion levels. This behaviour is observed to be the same in the columns within the same configurations as the corrosion level increases. Furthermore, the columns' ductility reduced with an increase in the confinement levels in all the columns [72–74].

The circular columns have a higher ultimate strain corresponding to the ultimate strength of the columns (Fig. 18(a-I, m-o)) than the square columns except in some of the lowly confined columns (Fig. 18(k and l)). This results from the uniform confinement of the circular columns which gives rise to a uniform stress distribution of the concrete along the cross-section [71,75–77]. In contrast, the square columns have their stress concentration at the edges which in some case led to the failure of the GFRP's.

5. Conclusion

Thirty RC column specimens with five different reinforcement corrosion levels and three confinement configurations were tested under cyclic compressive load. Moreover, the relationship between the seismic behaviour, such as rebar corrosion loss ratio, ultimate strength, normalised dissipated energy, and inelastic buckling of the rebar were investigated. The following conclusions can be drawn from this study.

- The circular columns have a higher axial cyclic load-carrying capacities which gradually decrease with increased corrosion and confinement than the square columns. The well confined circular columns (L/D = 5) have 41.32 MPa, 35.93 MPa, 32.04 MPa, 30.66 MPa and 25.92 MPa axial cyclic load carrying capacities for the 0%, 5%, 10%, 20% and 30% corrosion losses respectively. Meanwhile, the square columns with the same confinement and corrosion losses have 29.91 MPa, 25.98 MPa, 24.44 MPa, 22.48 MPa and 20.50 MPa axial cyclic load carrying capacities. A similar trend was observed in the medium confined and low confined columns. This results from the effectiveness of the transverse ties in the circular column, which has more significant confinement effectiveness coefficients than the square columns.
- The total energy dissipated by the RC columns reduced with increased levels of corrosion and confinement except in columns

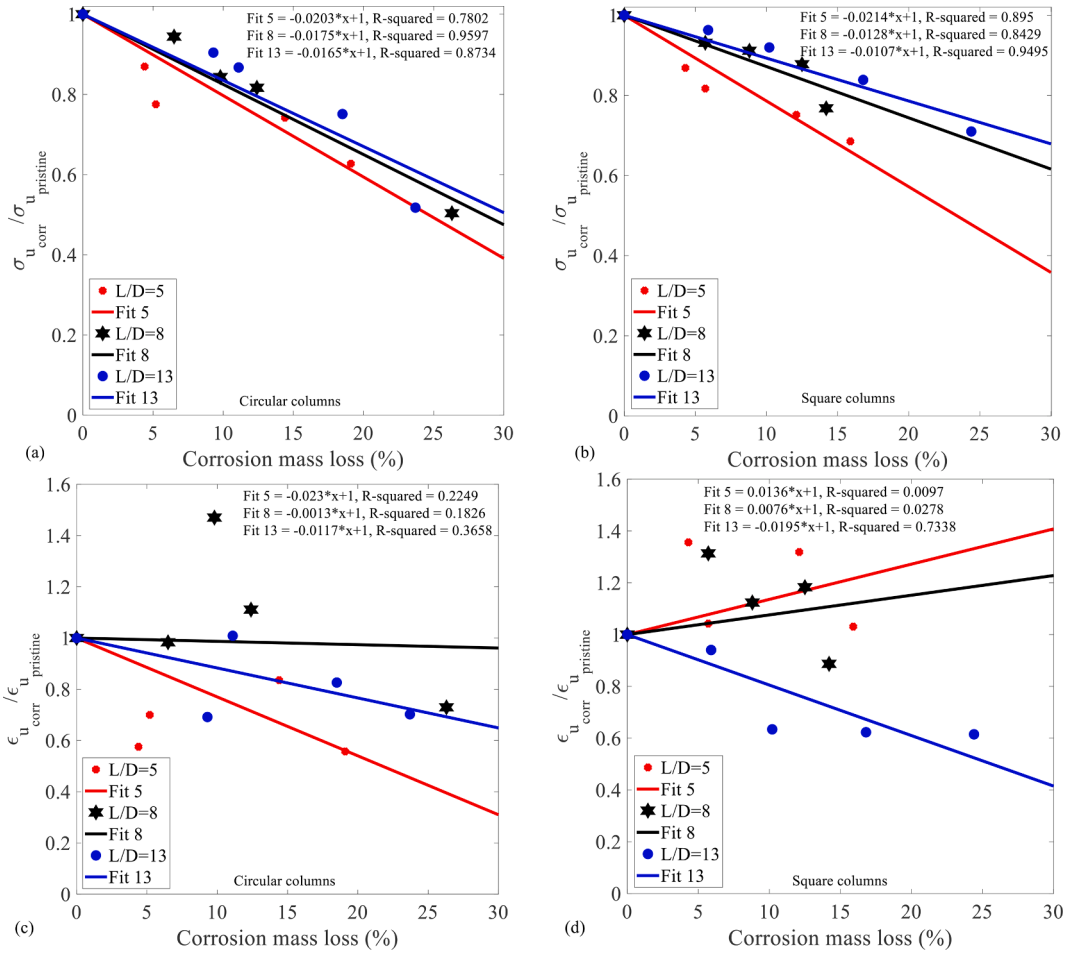

Fig. 17. The variation of stress and strain with corrosion of confined RC columns; strength (a-b) and strain (c-d).

with resuced acapacity due to failure of the GFRP ends. The energy disspated by the columns at the lower loading cycles are similar until after the 10th cycle when the circular columns have more energy disspated. This results from the ineffective confinement of the square columns in comparison to the circular columns within the same configuration.

- Corrosion of transverse confining steel affects the strength and deformability of confined concrete. The effectiveness of confinement reinforcements in confining the core concrete reduces as the corrosion increases. The strength of the highly confined circular column between the uncorroded and 30% corroded was decreased by about 37%, while the mediumly confined and lowly confined with the same corrosion mass loss were reduced by 50% and 48%, respectively.
- Transverse reinforcement showed much higher vulnerability to chloride-induced deterioration than the respective longitudinal reinforcement in the RC columns. Consequently, the ultimate strength of the columns reduced as corrosion damage increased and confinement effectiveness diminished. Well-confined specimens showed a lesser loss in strength and deformability after corrosion than under-confined specimens.
- With the strength and ductility losses experienced by old RC columns from the lack of adequate confinement and corrosion degradation, there is a need to improve their structural response with composite strengthening materials such as fibre-reinforced polymers and jacketing.

6. Author statement

Hammed O. Aminulai: Writing the paper, conducting the experimental testing and data analysis.

A. F. Robinson: Experimental officer supporting the first author in conducting the experimental testing.

Neil S. Ferguson: Editing the paper and supervising the first author.

Mohammad M. Kashani: lead supervisor, leading the research, supervising the student, and editing the paper.

Declaration of Competing Interest

The authors declare that they have no known competing financial interests or personal relationships that could have appeared to influence the work reported in this paper.

Data availability

Data will be made available on request.

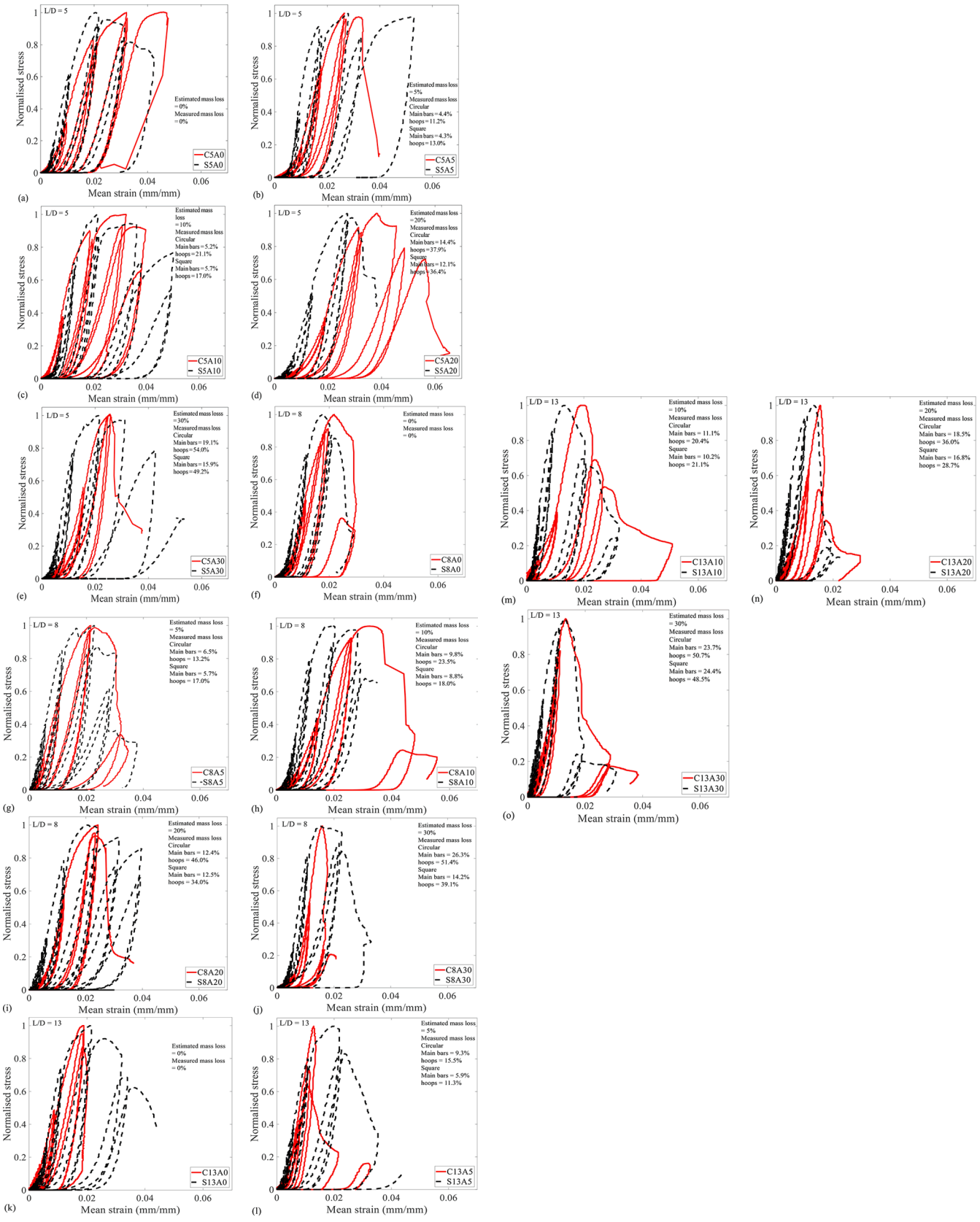

Fig. 18. Comparison of the normalised stress response of circular and square columns with varying corrosion and confinement levels; L/D = 5 (a-d), L/D = 8 (e-h) and L/D = 13(i-l).

References

[1] Chen J, et al. Compressive behavior of corroded RC columns strengthened with ultra-high performance jacket. Front Mater 2022;9(859620):1–14.
[2] Luo X, et al. Seismic behavior of corroded reinforced concrete column joints under low-cyclic repeated loading. Arch Civ Mech Eng 2020;20:40.
[3] Ma J, et al. Stress–strain model for confined concrete in rectangular columns with corroded transverse reinforcement. Eng Struct 2022;267(114710):1–14.
[4] Du YG, Clark LA, Chan AHC. Residual capacity of corroded reinforcing bars. Mag Concr Res 2005;57(3):135–47.
[5] Li Q, et al. Experimental study on seismic behaviors of concrete columns confined by corroded stirrups and lateral strength prediction. Constr Build Mater 2018;162:704–13.
[6] Vu NS, Yu B, Li B. Prediction of strength and drift capacity of corroded reinforced concrete columns. Constr Build Mater 2016;115:304–18.
[7] Biswas RK, et al. Effect of non-uniform rebar corrosion on structural performance of RC structures: a numerical and experimental investigation. Constr Build Mater 2020;230:116908.
[8] Akiyama M, Frangopol DM, Matsuzaki H. Life-cycle reliability of RC bridge piers under seismic and airborne chloride hazards. Earthq Eng Struct Dyn 2011;40(15):1671–87.
[9] Ou Y-C, Fan H-D, Nguyen ND. Long-term seismic performance of reinforced concrete bridges under steel reinforcement corrosion due to chloride attack. Earthq Eng Struct Dyn 2013;42(14):2113–27.
[10] Kashani, M.M., *Seismic Performance of Corroded RC Bridge Piers: Development of a Multi-Mechanical Nonlinear Fibre Beam-Column Model*. 2014.
[11] Kashani MM, et al. Impact of corrosion on low-cycle fatigue degradation of reinforcing bars with the effect of inelastic buckling. Int J Fatigue 2015;77:174–85.
[12] Kashani MM, Crewe AJ, Alexander NA. Nonlinear cyclic response of corrosion-damaged reinforcing bars with the effect of buckling. Constr Build Mater 2013;41:388–400.
[13] Kashani MM, Crewe AJ, Alexander NA. Use of a 3D optical measurement technique for stochastic corrosion pattern analysis of reinforcing bars subjected to accelerated corrosion. Corros Sci 2013;73:208–21.
[14] Lu C, et al. Mechanical properties of corroded steel bars in pre-cracked concrete suffering from chloride attack. Constr Build Mater 2016;123:649–60.
[15] Vu NS, Bing L. Seismic performance assessment of corroded reinforced concrete short columns. J Struct Eng 2018;144(04018018):1–12.
[16] Kashani MM, Maddocks J, Dizaj EA. Residual capacity of corroded reinforced concrete bridge components: state-of-the-art review. J Bridg Eng 2019;24(7):1–16.
[17] Ni Choine M, et al. Nonlinear dynamic analysis and seismic fragility assessment of a corrosion damaged integral bridge. Int J Struct Integrity 2016;7(2).
[18] Biondini F, Camnasio E, Palermo A. Lifetime seismic performance of concrete bridges exposed to corrosion. Struct Infrastruct Eng 2014;10(7):880–900.
[19] Akiyama, M. and D. Frangopol, M. , *Long-term seismic performance of RC structures in an aggressive environment: emphasis on bridge piers.* Structure and Infrastructure Engineering, 2014. **10**(7): p. 865-879 , year = 2014.
[20] Jia, J., et al., *Experimental investigation on the seismic performance of low-level corroded and retrofitted reinforced concrete bridge columns with CFRP fabric*, in *Engineering Structures*. 20p. 110225.
[21] Meda A, et al. Experimental evaluation of the corrosion influence on the cyclic behaviour of RC columns. Eng Struct 2014;76:112–23.
[22] Yuan W, Guo A, Li H. Seismic failure mode of coastal bridge piers considering the effects of corrosion-induced damage. Soil Dyn Earthq Eng 2017;93:135–46.
[23] Guo A, et al. Experimental investigation on the cyclic performance of reinforced concrete piers with chloride-induced corrosion in marine environment. Eng Struct 2015;105:1–11.
[24] Ma Y, Che Y, Gong J. Behavior of corrosion damaged circular reinforced concrete columns under cyclic loading. Constr Build Mater 2012;29:548–56.
[25] Yu L, et al. Structural performance of RC beams damaged by natural corrosion under sustained loading in a chloride environment. Eng Struct 2015;96:30–40.
[26] Ou Y-C, Nguyen ND. Influences of location of reinforcement corrosion on seismic performance of corroded reinforced concrete beams. Eng Struct 2016;126:210–23.
[27] Du, Y., L.A. Clark, and A. Chan, H. C. , *Impact of Reinforcement Corrosion on Ductile Behavior of Reinforced Concrete Beams.* ACI Structural Journal, 2007. **104**(3).
[28] Cairns J, Du Y, Law D. Structural performance of corrosion-damaged concrete beams. Magaz Concr Res - MAG CONCR RES 2008;60:359–70.
[29] El-Sayed AK, Hussain RR, Ahmed BS. Influence of stirrup corrosion on shear strength of reinforced concrete slender beams. ACI Struct J 2016;113(6).
[30] Azad A, Ahmad S, Algohi B. Flexural strength of corroded reinforced concrete beams. Magaz Concr Res - MAG CONCR RES 2010;62:405–14.
[31] Dang VH, François R. Influence of long-term corrosion in chloride environment on mechanical behaviour of RC beam. Eng Struct 2013;48:558–68.
[32] Jnaid F, Aboutaha RS. Residual flexural strength of corroded reinforced concrete beams. Eng Struct 2016;119:198–216.
[33] Goksu C, Ilki A. Seismic behavior of reinforced concrete columns with corroded deformed reinforcing bars. ACI Struct J 2016;113(5):1053–64.
[34] Yang S-Y, et al. Experimental research on hysteretic behaviors of corroded reinforced concrete columns with different maximum amounts of corrosion of rebar. Constr Build Mater 2016;121:319–27.
[35] Li P, et al. Experimental study on the mechanical properties of corroded RC columns repaired with large rupture strain FRP. J Build Eng 2022;54:104413.
[36] Meda A, et al. Corroded RC columns repair and strengthening with high performance fiber reinforced concrete jacket. Mater Struct 2016;49(5):1967–78.
[37] Rajput AS, Sharma UK. Seismic behavior of under confined square reinforced concrete columns. Structures 2018;13:26–35.
[38] Li Q, et al. Effects of reinforcement corrosion and sustained load on mechanical behavior of reinforced concrete columns. Materials (Basel) 2022;15(10).
[39] Dai K-Y, Lu D-G, Yu X-H. Experimental investigation on the seismic performance of corroded reinforced concrete columns designed with low and high axial load ratios. J Build Eng 2021;44:102615.
[40] Matthews B, Palermo A, Scott A. Overview of the cyclic response of reinforced concrete members subjected to artificial chloride-induced corrosion. Struct Concr 2022.
[41] Zongjin Li, et al., *Advanced Concrete Technology*. 2nd ed. 2022. i-xii.
[42] Choi MH, Lee CH. Seismic behavior of existing reinforced concrete columns with non-seismic details under low axial loads. Materials (Basel) 2022;15(3).
[43] Apostolopoulos C, Konstantopoulos G, Koulouris K. Seismic resistance prediction of corroded S400 (BSt420) reinforcing bars. Int J Struct Integrity 2018;9(1):119–38.
[44] Rajput AS, Sharma UK. Corroded reinforced concrete columns under simulated seismic loading. Eng Struct 2018;171:453–63.
[45] Basdeki M, Koulouris K, Apostolopoulos C. Effect of corrosion on the hysteretic behavior of steel reinforcing bars and corroded RC columns. Appl Sci 2022;12(15):7451.
[46] Yang H, Sun P, Deng Y. Experiment investigation of the influence of reinforcing bar buckling on seismic behavior of RC columns. Eng Struct 2020;220:110923.
[47] Kashani MM, et al. Nonlinear fibre element modelling of RC bridge piers considering inelastic buckling of reinforcement. Eng Struct 2016;116:163–77.
[48] Kashani MM, et al. Non-linear flexural behaviour of RC columns including bar buckling and fatigue degradation. Mag Concr Res 2018;70(5):231–47.
[49] Nojavan A, Schultz AE, Chao S-H. Analytical study of in-plane buckling of longitudinal bars in reinforced concrete columns under extreme earthquake loading. Eng Struct 2017;134:48–60.
[50] Kashani MM, et al. Computational modelling strategies for nonlinear response prediction of corroded circular RC Bridge Piers. Adv Mater Sci Eng 2016;2016:2738265.
[51] Su J, et al. Influence of reinforcement buckling on the seismic performance of reinforced concrete columns. Eng Struct 2015;103:174–88.
[52] The British Standards, *Steel for the reinforcement of concrete — Weldable reinforcing steel — General*, in *BS EN 10080:2005*. 2005, BSI Standards Limited: London, UK.
[53] The British Standards, *Steel for the reinforcement of concrete — Weldable reinforcing steel — Bar, coil and decoiled product — Specification*, in *BS 4449-2005+A3-2016*. 2016, BSI Standards Limited: London, UK.
[54] The British Standards, *Metallic materials — Tensile testing, Part 1: Method of test at room temperature*, in *BS EN ISO 6892–1:2019*. 2020, BSI Standards Limited: London, UK.
[55] Kashani MM, Crewe AJ, Alexander NA. Nonlinear stress–strain behaviour of corrosion-damaged reinforcing bars including inelastic buckling. Eng Struct 2013;48:417–29.
[56] Yuan Y, Ji Y, Shah SP. Comparison of two accelerated corrosion techniques for concrete structures. ACI Struct J 2007;104(3):344–7.
[57] Shen D, et al. Seismic performance of corroded reinforced concrete beam-column joints repaired with BFRP sheets. Constr Build Mater 2021;307:124731.
[58] Hou L, et al. Corrosion behavior and flexural performance of reinforced concrete/ultrahigh toughness cementitious composite (RC/UHTCC) beams under sustained loading and shrinkage cracking. Constr Build Mater 2019;198:278–87.
[59] Mak MWT, Desnerck P, Lees JM. Corrosion-induced cracking and bond strength in reinforced concrete. Constr Build Mater 2019;208:228–41.
[60] Almusallam AA. Effect of degree of corrosion on the properties of reinforcing steel bars. Constr Build Mater 2001;15(8):361–8.
[61] ASTM, G.-. Standard practice for preparing, cleaning, and evaluating corrosion test specimens,. 2011, ASTM International.
[62] Apostolopoulos CA, Papadopoulos MP. Tensile and low cycle fatigue behavior of corroded reinforcing steel bars S400. Constr Build Mater 2007;21(4):855–64.
[63] Apostolopoulos CA, Papadopoulos MP, Pantelakis SG. Tensile behavior of corroded reinforcing steel bars BSt 500s. Constr Build Mater 2006;20(9):782–9.
[64] Instron, *WAVEMATRIX2*. 2018, Illinois Tool Works Inc.: Illinios, US.
[65] Gu X-L, et al. Corrosion of stirrups under different relative humidity conditions in concrete exposed to chloride environment. J Mater Civ Eng 2020;32(1):04019329.
[66] Nguyen CV, Lambert P. Effect of current density on accelerated corrosion of reinforcing steel bars in concrete. Struct Infrastruct Eng 2018;14(11):1535–46.
[67] Ou Y-C, Tsai L-L, Chen H-H. Cyclic performance of large-scale corroded reinforced concrete beams. Earthq Eng Struct Dyn 2012;41(4):593–604.
[68] Kashani MM. Size effect on inelastic buckling behavior of accelerated pitted corroded bars in porous media. J Mater Civ Eng 2017;29(7):04017022.
[69] Kashani MM, et al. Phenomenological hysteretic model for corroded reinforcing bars including inelastic buckling and low-cycle fatigue degradation. Comput Struct 2015;156:58–71.
[70] Vu NS, Yu B, Li B. Stress-strain model for confined concrete with corroded transverse reinforcement. Eng Struct 2017;151:472–87.

[71] Liang X, Sritharan S. Effects of confinement in circular hollow concrete columns. J Struct Eng 2018;144(9):04018159.
[72] Saatcioglu M, Razvi SR. Strength and ductility of confined concrete. J Struct Eng 1992;118(6):1590–607.
[73] Mander JB, Priestley MJN, Park R. Theoretical stress-strain model for confined concrete. J Struct Eng 1988;114(8):1804–26.
[74] Hoshikuma J, et al. Stress-strain model for confined reinforced concrete in Bridge Piers. J Struct Eng 1997;123(5):624–33.
[75] Liang X, Beck R, Sritharan S. Understanding the Confined Concrete Behavior on the Response of Hollow Bridge Columns. Department of Civil Construction and Environmental Engineering. Iowa State University; 2015.
[76] Ayough P, et al. The effects of cross-sectional shapes on the axial performance of concrete-filled steel tube columns. J Constr Steel Res 2021;176:106424.
[77] Colajanni P, Fossetti M, Macaluso G. Effects of confinement level, cross-section shape and corner radius on the cyclic behavior of CFRCM confined concrete columns. Constr Build Mater 2014;55:379–89.